Aerodynamic aspects of the sealing of gas-turbine rotor-stator systems

Part 2: The performance of simple seals in a quasi-axisymmetric external flow

U. P. Phadke
Scientific Generics, King's Court, Cambridge CB4 2PF, UK

J. M. Owen
School of Engineering and Applied Sciences, University of Sussex, Falmer, Brighton, Sussex BN1 9QT, UK

Received 3 April 1987 and accepted for publication on 29 June 1987

The sealing characteristics of a shrouded rotor-stator system with an external flow of air have been studied using flow visualization, pressure, and concentration measurements. Three shroud geometries, incorporating axial clearance or radial clearance seals, have been tested for a range of clearance ratios for both rotational and axial Reynolds numbers Re_θ and Re_w respectively, up to 1.2×10^6. It was found that there were two regimes: a rotation-dominated regime at low values of Re_w/Re_θ, and an external-flow-dominated regime at high values. For $Re_w=0$, $C_{w,min}$ (the dimensionless flow rate of sealing air necessary to prevent the ingress of external fluid into the rotor-stator wheel space) increased with increasing Re_θ. For small values of Re_w/Re_θ, $C_{w,min}$ decreased with increasing Re_w; for large values of Re_w/Re_θ, $C_{w,min}$ was proportional to Re_w and was independent of Re_θ. The latter effect is attributed to the nonaxisymmetric pressure distribution in the external flow: fluid moved transversely across the wheel space from high-pressure to low-pressure regions of the external flow.

Keywords: sealing; rotating disks; rotor-stators

Introduction

In Part 1 (Parts 1 and 3, Refs. 1 and 2, are respectively referred to as I and III) of this series of three papers, a shrouded rotor-stator system with seven different seal geometries was tested in a quiescent environment: the air outside the system was stationary. It was found that $C_{w,min}$, the dimensionless flow rate of cooling air necessary to prevent the ingress of external fluid into the wheel space, increased with increasing seal clearance and with increasing rotational speed.

Figure 1 shows the three seals (seals 1, 3, and 5 from I), tested in the presence of an external axial flow of air, that are the subject of this paper. The axial flow was supplied through an annulus in an attempt to model the mainstream gas flow that occurs inside gas-turbine rotors. In the real engine the mainstream gas is much hotter than the cooling air in the wheel space, and the blades and nozzles can create swirl and circumferential variations in both velocity and pressure. In the model tested, the cooling air and external flows were at similar temperatures, and there was no deliberate attempt to create swirl or circumferential variations in the flow. However, as described below, it was not possible to achieve complete axisymmetry, and the relatively small nonaxisymmetric pressure variations gave rise to some interesting effects.

The external-flow rig and instrumentation are described in the second section, and preliminary tests with seal 1 are discussed in the third section. In the fourth and fifth sections, the criteria for the determination of ingress and the performance of the three seals are discussed.

Experimental apparatus

The external-flow rotor-stator rig comprised a shrouded rotor-stator system with a surrounding annular external-flow channel, and a simplified diagram is shown in Figure 2. Only the salient features of the rig and the associated instrumentation are described below; further details are given in Ref. 3.

External-flow rotor-stator rig

The rotor was of composite construction with a peripheral shroud clamped between two aluminum disks. The nominal outside diameter of the shroud was 376 mm (this was varied for

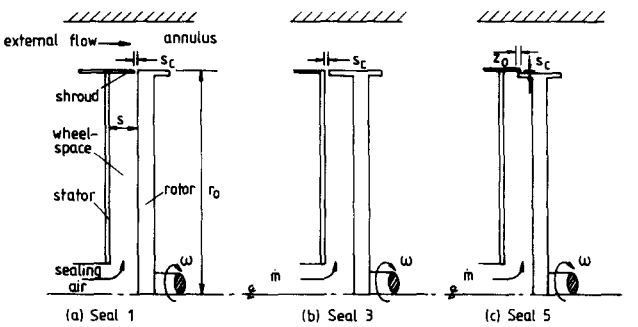

Figure 1 Simplified diagram of the three seals tested: (a) seal 1; (b) seal 2; (c) seal 3

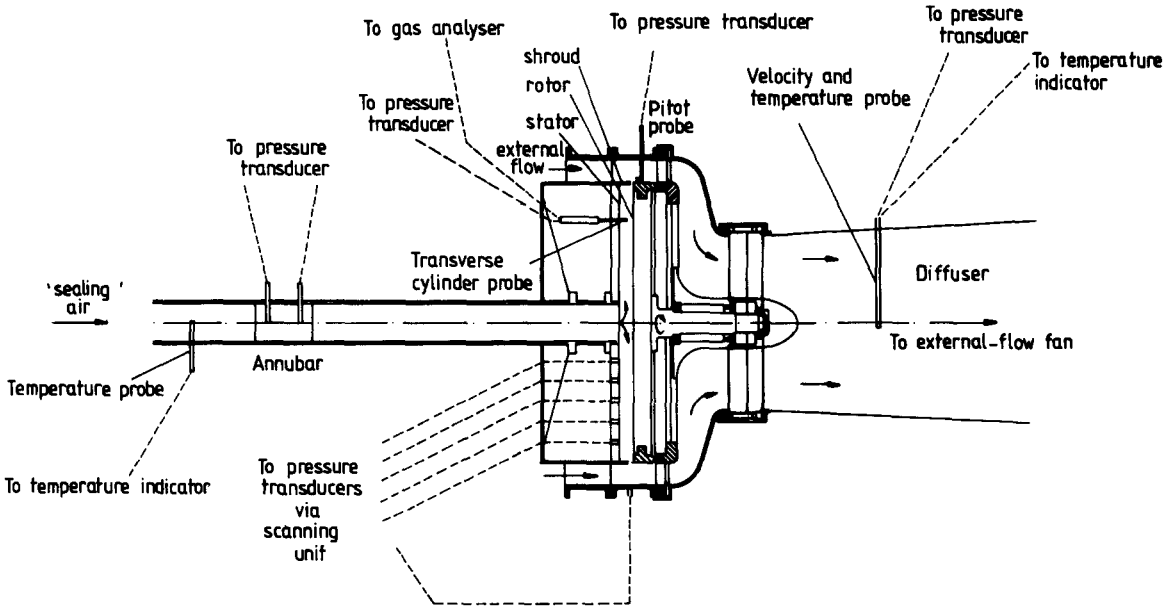

Figure 2 Schematic diagram of external-flow rotor-stator rig and instrumentation

seal 5), and the axial thickness of the composite rotor was 12.5 mm. The rotor could be spun up to 5000 r/min by a 5-kW electric motor, and the speed was measured to an accuracy of one r/min.

The stator was made from a transparent polycarbonate disk of 374 mm diameter and 9 mm thickness supported by aluminum rings and radial stiffeners, and a peripheral perspex shroud 2 mm thick was attached to the outside of the stator. As the direction of the external flow was axially from the stator toward the rotor, the outside diameter of the stator (378 mm) was made larger than that of the rotor (376 mm) to reduce impingement of the flow at the periphery of the rotor.

Although, for some of the tests, the axial gap s between the rotor and stator was varied, the gap ratio for most tests was maintained at $GH \simeq 0.1$. For seal 1 (the datum seal), the axial clearance, s_c, was varied by moving the peripheral shroud on the stator; for seal 3, s_c was varied by moving the whole stator assembly (as s_c was only changed from 0.9 to 3.8 mm, the resulting variation in G was unlikely to be important). For seal 5, rotating shrouds of different outside diameters were used to produce radial clearances of either 0.9 mm or 1.9 mm; the radial thickness of the rotating shroud was approximately 5 mm, and the axial widths of the rotating and stationary shrouds were 10.5 mm, which resulted in an overlap of $z_o = 2$ mm ($H = 0.01$).

To form the external-flow annulus, the rotor and stator were enclosed inside a stationary cylinder, made from 5-mm-thick perspex, with an inside diameter of 438 mm and an axial length of 120 mm, giving a radial channel height of $h = 30$ mm. The inlet end of the annulus was located approximately 90 mm from the upstream face of the rotor, and the exit end was fitted to a

Nomenclature

C_{ij}	Ingress constant
C_w	$\dot{m}/\mu r_o$, mass flow coefficient
G	s/r_o, gap ratio
G_c	s_c/r_o, seal clearance ratio
h	Radial height of annulus
H	z_0/r_o, seal overlap ratio
$\dot{m}$	Mass flow rate of sealing air
p	Static pressure
p^*	$10^3(p-p_a)/p_a$, dimensionless pressure drop
r	Radial distance from disk centerline
r_o	Outer radius of disk
Re_θ	$\rho\omega r_o^2/\mu$, rotational Reynolds number
Re_w	$\rho\bar{W}r_o/\mu$, axial flow Reynolds number
s	Axial gap between rotor and stator
s_c	Seal clearance
V_r, V_θ, V_z	Radial, tangential, and axial components of velocity
W	Axial component of velocity in the external-flow annulus
$\bar{W}$	Uniform value of W in inner part of annulus
x	r/r_o dimensionless radius
z	Axial distance measured from stator face
z_o	Axial overlap of radial clearance seals
Δr	Radial distance from inner wall of annulus
μ	Fluid viscosity
ρ	Fluid density
ω	Angular speed of rotor
η	Volumetric concentration (ratio of volumetric flow rates of nitrous oxide and air)

Subscripts

a	Ambient conditions
c	Sealing flow
min	Minimum value to prevent ingress
r	Rotor
s	Stator
1, 2	Outer and inner shrouds

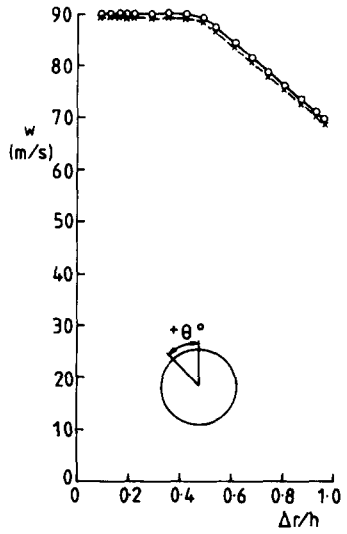

Figure 3 Radial variation of the axial component of velocity in the annulus: —— ○ ——, $\theta=0°$; —— × ——, $\theta=90°$

fiberglass molding. This molding conveyed the external flow from the annulus to a conical diffuser, which was connected to the inlet of a centrifugal fan.

The external-flow fan, which was operated in the suction mode, could produce flow rates up to 3.2 m^3/s at a differential head of 700 mm WG. The sealing-air flow was supplied from a separate fan capable of flow rates up to 0.15 m^3/s at 1100 mm WG. The outlet from the sealing-air fan was connected to a hole, of 50 mm diameter, in the center of the stator by a steel pipe 760 mm long and 50 mm inside diameter.

Instrumentation

The sealing-air flow rate was measured, to an accuracy of $\pm 3\%$, by means of an Annubar differential-pressure device fitted in the pipe between the fan and the stator. The differential pressure was measured with a Furness Controls five-range micromanometer, with an accuracy of $\pm 1\%$ FSD on each of the ranges.

Pressure taps, with an inside diameter of 0.5 mm, were fitted to the stator and to the outer wall of the annulus. On the stator, the taps were fitted at 12 radial locations (53 mm $\leqslant r \leqslant$ 183 mm) for one angular position and at 21 angular locations for one radial position ($r=183$ mm). On the outer wall of the annulus, taps were fitted at 27 angular locations for one axial position (corresponding to the plane of the upstream face of the rotor). Referring to Figure 3 for the definition of θ, we see that the 27 angular locations were at $\theta=0$, 15°, 30°, 45°, 60°, 75°, 85°, 90°, 95°, 105°, 120°, 135°, 150°, 165°, 180°, 195°, 205°, 210°, 215°, 225°, 240°, 300°, 315°, 325°, 330°, 335°, and 345°. The static pressures were measured by one of two multirange Mercury micromanometers, with maximum ranges of 30 mm and 1000 mm WG, respectively, and an accuracy of $\pm 1\%$ FSD for each range.

The axial component of velocity in the external-flow annulus was measured by a pitot tube (located at either $\theta=0°$ or 90°), and the radial and tangential components of velocity in the wheel space between the rotor and stator were determined by a two-hole transverse-cylinder probe. This probe was positioned by traversing gear, activated from a stepper motor, with axial and angular position accuracies of ± 0.1 mm and $\pm 0.1°$, respectively. The pressures from the pitot tube and cylinder probe were measured by one of the mercury micromanometers.

Concentration measurements in the wheel space were used to determine the degree of mixing between the sealing air and the external flow, one of which was seeded with around 100 ppm of nitrous oxide. A small pump was used to extract a sample of fluid through one of the two holes of the cylinder probe (the hole being aligned with the direction of the flow). The concentration was measured by a two-range GP Instrumentation infrared gas analyzer (IRGA), which had an accuracy of ± 1 ppm on the range used. The sampling rate could be adjusted to produce isokinetic conditions at the probe, but tests in nonswirling flows suggested that the sampling rate could be increased to four times the isokinetic value before errors in concentration measurement exceeded $\pm 3\%$. The temperatures of the nitrous oxide, the coolant, and the external flow were measured using thermocouples in standard total-temperature probes.

Flow visualization was carried out with the aid of a Spectra-Physics 4-W Ar-ion laser and a Concept smoke generator. A cylindrical lens was used to create slit illumination of an r-z plane in the wheel space and the external-flow annulus. Micron-sized oil particles, produced by the smoke generator, were injected into the inlet of either the annulus or the sealing-air fan.

Preliminary tests with seal 1

Before attempting to quantify $C_{w,min}$, we made preliminary tests to examine the flow structure using velocity, pressure, and concentration measurements as well as flow visualization.

Tests in the stationary system

The axial component of velocity, W, in the external-flow annulus was measured at the plane of the upstream face of the rotor. Figure 3 shows that the radial variation of W was uniform over the inner half of the annulus, but the flow as sheared in the outer half. The shear was caused by separation of the incoming flow, and the symbol $\bar{W}$ is used below to refer to the value of W in the inner part of the annulus.

It was also found that, however much care was taken in aligning the annulus, it was not possible to achieve axisymmetric flow. Figure 4 shows the circumferential variation of static pressure difference $(p-p_a)$ on the outer wall of the annulus, in the plane of the upstream face of the rotor, for a range of different values of $\bar{W}$. Also shown is the circumferential variation of $(p-p_a)/\frac{1}{2}\rho\bar{W}^2$, the average of which is approximately -1. The maximum circumferential pressure difference between any two of the 27 taps was approximately 7% of the dynamic pressure, $\frac{1}{2}\rho\bar{W}^2$. Since this was the closest to axisymmetric flow that could be achieved, it is referred to here as "quasi-axisymmetric flow."

As a result of the nonaxisymmetric pressure distribution in the external flow, ingress could occur even when the rotor was stationary. Flow visualization showed that fluid moved transversely across the wheel space from the high- to the low-pressure regions in the annulus, and typical flow patterns are shown in Figure 5 for seal 1 with $G_c=0.01$ and $Re_w=0.21\times10^6$. The amount of ingested fluid decreased with increasing C_w until, at $C_w\simeq1800$, there was little sign of ingress.

Concentration measurements in the rotating system

Figure 6 shows the axial variation of $(\eta-\eta_c)/\eta_c$ (where η and η_c are the volumetric concentrations of nitrous oxide in the wheel space and in the sealing air at inlet to the system, respectively) at $x=0.81$ for seals 3 and 5 with $G_c=0.01$, $Re_w=1.17\times10^6$, $C_w=2500$, and $Re_\theta/10^6=0.5$ and 1.0. A negative value of $(\eta-\eta_c)/\eta_c$ indicates that ingress has occurred, which is the case

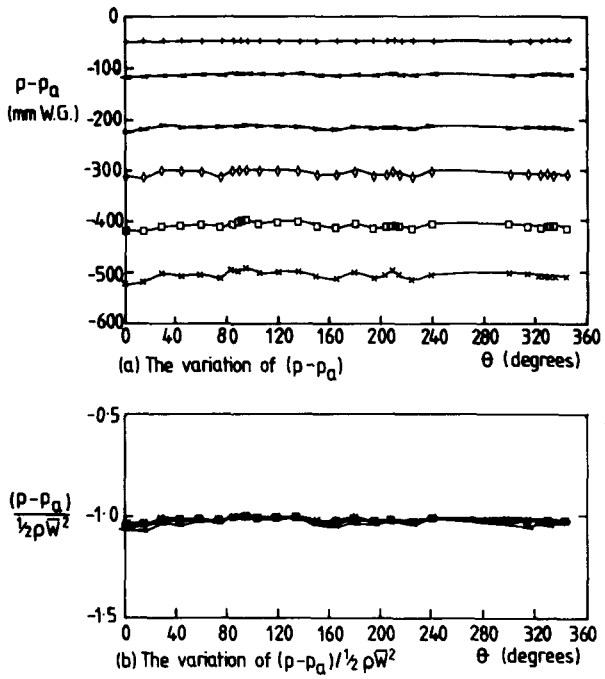

Figure 4 The effect of external flow on the circumferential variation of static pressure in the annulus: (a) the variation of $p-p_a$; (b) the variation of $(p-p_a)/\frac{1}{2}\rho\bar{W}^2$

Symbol	+	◁	▷	◇	□	×
$\bar{W}$ (m/s)	27	42	58	69	80	89
$Re_w/10^6$	0.36	0.54	0.72	0.89	1.06	1.19

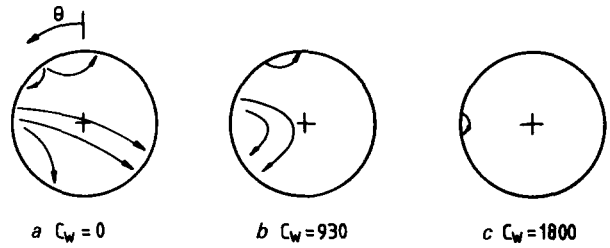

Figure 5 Observed flow patterns in the wheel space for seal 1 with $G_c=0.01$, $Re_\theta=0$, $Re_w=0.21\times10^6$: (a) $C_w=0$; (b) $C_w=930$; (c) $C_w=1800$

for all the data in Figure 6. It can also be seen that the minimum concentration occurs near the stator where $(\eta-\eta_c)/\eta_c\simeq-1$, which suggests that the flow in the stator boundary layer at this radius consists almost entirely of ingested fluid. Also as $(\eta-\eta_c)/\eta_c<0$ near the rotor, some of the ingested fluid has penetrated into the boundary layer on the rotor. However, although there is a significant difference in the concentration distributions for the two seals, the distribution appears to be little affected by rotational speed.

The concentration measurements with external flow are in marked contrast to those without (see Figure 10 in I). Without external flow, concentration levels for equivalent conditions were considerably higher: the *minimum* value of concentration measured for $Re_w=0$ was larger than the *maximum* value for $Re_w=1.17\times10^6$. Also, without external flow there was no sign of ingested fluid near the rotor for $x=0.81$, and the concentration level decreased significantly with increasing Re_θ. In particular, there was no sign of ingress for seal 5 with $G_c=0.01$, $C_w=2850$, and $Re_\theta=0.5\times10^6$ when $Re_w=0$.

Criteria for the determination of ingress

Pressure criterion

Pressure measurements provide indirect evidence of ingress: if the pressure in the wheel space is less than that outside, then it is assumed that ingress occurs. In earlier tests without external flow, the radially outermost pressure tap was used: negative pressure (relative to that of the surrounding air) was assumed to indicate ingress, and zero pressure was used as the criterion for sealing.

For the tests with external flow, the pressure difference between the outermost tap on the stator (at $r/r_0=0.97$) and the corresponding tap on the outer wall of the external-flow annulus was measured for each of the 21 pairs of pressure taps. As discussed, the external flow was nonaxisymmetric, and so the arithmetic mean of these pressure differences, $\overline{\Delta p}$, was used to determine ingress: $C_{w,min}$ was based on the flow rate for which $\overline{\Delta p}$ was zero.

The "$\overline{\Delta p}$ pressure criterion" is arbitrary, and other pressure criteria may be more appropriate. For example, other pressure taps could have been used, or the maximum rather than the arithmetic mean might be more appropriate. In fact, tests were conducted in which the penultimate pressure tap on the stator was used, and other tests were carried out using the maximum pressure difference. However, the $\overline{\Delta p}$ criterion appeared to produce the best correlation with the flow visualization, which is discussed below.

Flow visualization criterion

Oil particles from the smoke generator were introduced into the external flow, and the wheel space was illuminated with the Ar-ion laser. The rotational speed and the external flow rate were kept constant, and the flow rate of the sealing air was increased until no smoke was observed to enter the wheel space. This flow rate was used to calculate $C_{w,min}$.

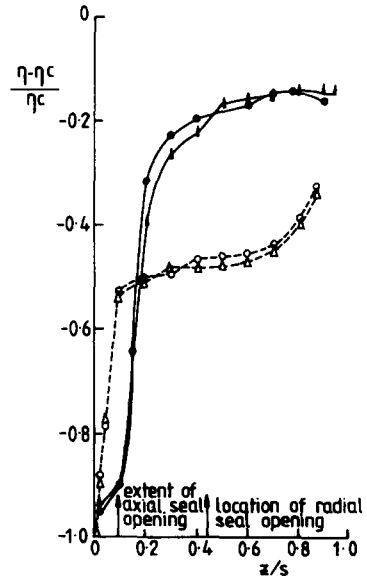

Figure 6 The effect of Re_θ on the axial variation of concentration for $x=0.81$, $G_c=0.01$, $C_w=2500$, and $Re_w=1.17\times10^6$. $Re_\theta=0.5\times10^6$: —○—, seal 3; —●—, seal 5; $Re_\theta=10^6$: —△—, seal 3; —▲—, seal 5

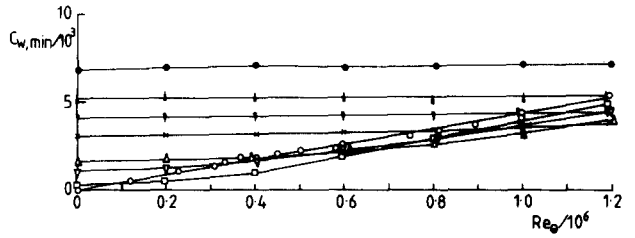

Figure 7 The effect of Re_w on the variation of $C_{w,min}$ with Re_θ for seal 1 with $G_c=0.005$

Symbol	○	□	▽	△	×	▼	▲	●
$Re_w/10^6$	0	0.05	0.20	0.33	0.54	0.78	0.94	1.16

Concentration criterion

If the sealing air is seeded with nitrous oxide, the results discussed in the previous section show that, when ingress occurs, the concentration is reduced near the stator. For the ingress tests reported below, the external air was seeded with approximately 100 ppm of nitrous oxide, and the cooling air was unseeded (the inlet of the sealing-air fan was located outside the laboratory to avoid contamination). The two-hole cylinder probe was used to extract samples from the wheel space at a fixed location ($x=0.81$, $z/s=0.02$), and the cooling-air flow rate was adjusted (for constant values of external flow rate and rotational speed) until the measured concentration was approximately 1 ppm. This flow rate was then used to calculate $C_{w,min}$.

Observations

Each technique has advantages and disadvantages. Pressure measurements are simple to make but provide only indirect evidence of ingress. Flow visualization provides a direct indication of ingress, but it is difficult to use the technique at large flow rates. Concentration measurements give a direct measure of ingress at one point in the wheel space, but the measurements are time-consuming and difficult to make in the unsteady conditions that prevail at large external flow rates. Collectively, the three techniques are helpful in giving an overall picture of the ingress problem, and, although there are quantitative differences between them, they all produce the same qualitative results.

It should be emphasized, however, that these techniques provide an estimate of the sealing-air flow rate necessary to prevent "incipient ingress": that is, the flow rate that just prevents any external fluid from entering the wheel space. If, in an engine, hot mainstream gas is ingested into the wheel space, there may not be a serious problem until the rotor starts to overheat. "Significant ingress" occurs when the rotor first experiences the effect of the ingested fluid: its detection is beyond the scope of this paper.

Sealing performance

Variation of $C_{w,min}$ with Re_θ for the datum axial clearance seal (seal 1)

Figure 7 shows the variation of $C_{w,min}$, measured using the flow visualization technique, with Re_θ for eight different values of Re_w for seal 1 with $G_c=0.005$.

For $Re_w=0$, $C_{w,min} \propto Re_\theta$, and the correlation of the data is within 5% of that obtained from earlier tests in the absence of external flow (see Equation 5 of I). However, for large values of Re_w ($Re_w>0.5\times10^6$), $C_{w,min}$ is virtually independent of Re_θ: this is consistent with the findings of Abe *et al.*[4]. At intermediate values of Re_w ($0<Re_w<0.5\times10^6$), $C_{w,min}$ is independent of rotational speed at small values of Re_θ but it is proportional to rotational speed at large values of Re_θ (where the value of $C_{w,min}$ is actually less than that required in the absence of external flow).

Similar results were obtained for $G_c=0.01$ and 0.02, and $C_{w,min}$ increased with increasing G_c. Also, the trends observed using flow visualization were confirmed by pressure and concentration measurements, as shown in Figure 8 for $G_c=0.01$. The quantitative differences between the values of $C_{w,min}$ obtained from the three criteria are most significant for $Re_w>0$: the concentration measurements give values of $C_{w,min}$ slightly higher than those obtained using the flow visualization criterion, and the pressure measurements are about 20% higher. For $Re_w=0$, the pressure and flow visualization criteria produce similar results, and the concentration criterion produces slightly lower values of $C_{w,min}$.

Despite the quantitative differences between the three criteria, the results provide evidence of two distinct regimes: a rotation-dominated regime where, at relatively small values of Re_w, $C_{w,min} \propto Re_\theta$; and an external-flow-dominated regime where, at relatively large values of Re_w, $C_{w,min}$ is virtually independent of Re_θ. It can also be seen from Figure 8 that the external flow increases $C_{w,min}$ (compared with the results for $Re_w=0$) at low values of Re_θ and decreases it (for moderate external-flow rates) at high values of Re_θ.

Variation of $C_{w,min}$ with Re_w for seal 1

Figure 9 shows the variation of $C_{w,min}$, determined using flow visualization, with Re_w for the case where the rotor is stationary. It can be seen that $C_{w,min}=cRe_w$, and the values of c, the constant of proportionality, are 0.0059, 0.0085, and 0.0130 for $G_c=0.005$, 0.01, and 0.02, respectively. Using the pressure criterion, the three values of c were found to be 0.0075, 0.0102, and 0.0158; concentration measurements were made at $G_c=0.01$ for which $c=0.0090$.

The pressure asymmetry is related to Re_w: the two effects were inseparable for all the measurements reported in this paper, and so correlation with Re_w implies correlation with pressure asymmetry. In III, where the pressure asymmetry and the external flow rate are separated, it is shown that ingress is caused by the asymmetry rather than by Re_w itself.

Figure 10(a), (b), and (c) show the variation of $C_{w,min}$ with Re_w for $G_{w,min}=0.005$, 0.01, an 0.02 over the Reynolds number range $0\leqslant Re_\theta\leqslant1.2\times10^6$. The data points were obtained using flow

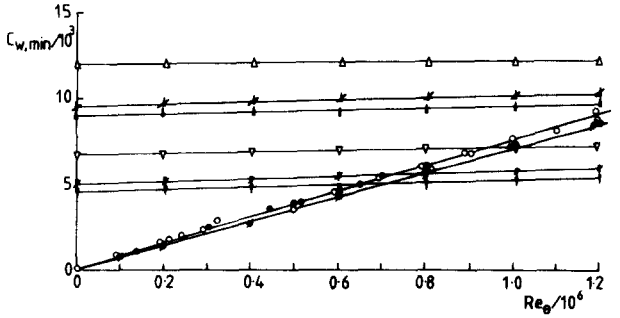

Figure 8 The variation of $C_{w,min}$ with Re_θ for seal 1 with $G_c=0.01$ according to the three ingress criteria

$Re_w/10^6$	0	0.59	1.15
Δp pressure criterion	○	▽	△
Flow visualization criterion	●	▼	▲

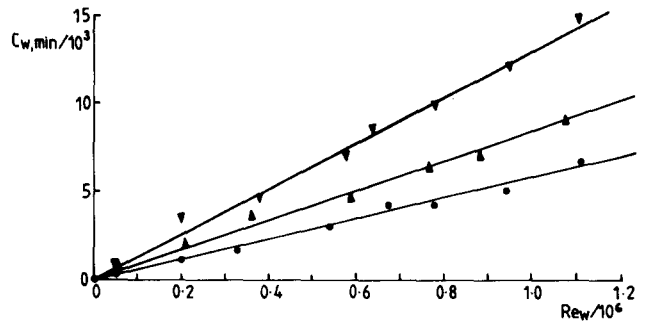

Figure 9 The effect of G_c on the variation of $C_{w,min}$ with Re_w for seal 1 with $Re_\theta=0$ (according to the flow visualization criterion).

Symbol	●	▲	▼
G_c	0.005	0.01	0.02

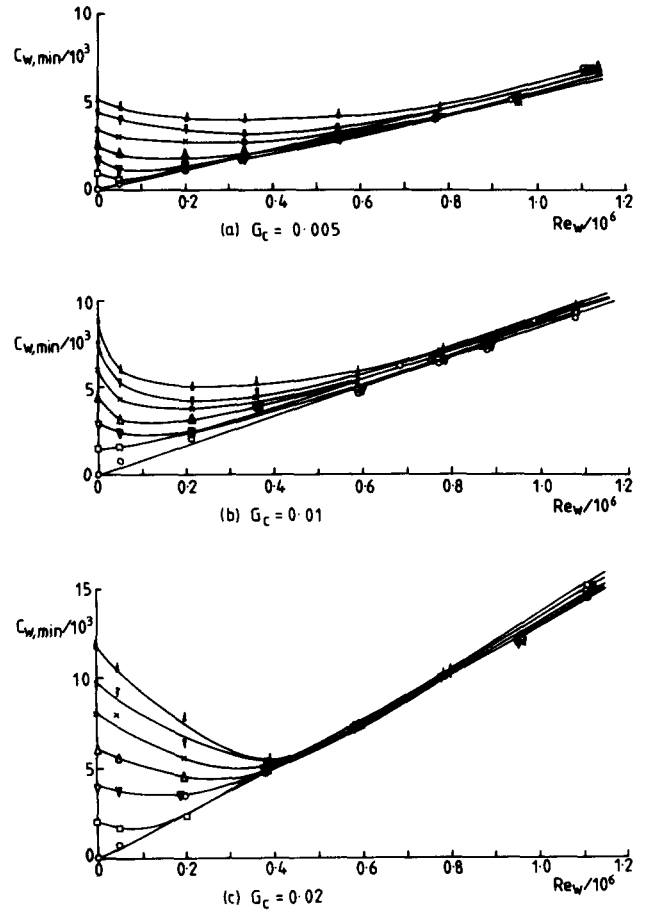

Figure 10 The effect of Re_θ on the variation of $C_{w,min}$ with Re_w for seal 1 (according to the flow visualization criterion): (a) $G_c=0.005$; (b) $G_c=0.01$; (c) $G_c=0.02$

Symbol	○	□	▽	△	×	▼	▲
$Re_\theta/10^6$	0	0.2	0.4	0.6	0.8	1.0	1.2

visualization, and the curves were produced from a least-squares regression fit to all the data points for each value of G_c.

Referring to Figure 10(a) for $G_c=0.005$, for $Re_w/Re_\theta \leqslant 0.3$, $C_{w,min}$ decreases with increasing Re_w. This effect can be explained by considering the flow in the vicinity of the seal. Vaughan[5] obtained numerical solutions of the elliptic equations of motion for turbulent flow in a rotor-stator system with $G_c=0.01$, $C_w=10^3$, $Re_\theta=8\times10^5$, and $0\leqslant Re_w\leqslant 6\times10^5$. His computed streamlines showed that fluid ingested into the wheel space from the external flow tends to separate from the edge of the shroud, and the resulting separation bubble reduces the effective clearance between the shroud and the rotor. For axisymmetric flow, the separation bubble grows in size with increasing external-flow rate, and $C_{w,min}$ is decreased.

Under nonaxisymmetric conditions, external flow can impinge on the rotor at some angular locations. This results in radial inflow at these locations and outflow at others, with fluid moving transversely across the wheel space from regions of high to low pressure in the annulus. Unlike the axisymmetric case, a nonaxisymmetric flow tends to create an increase of $C_{w,min}$ with increasing Re_w. There is, therefore, a minimum value of $C_{w,min}$ at the point where the axisymmetric sealing effect of the external flow is balanced by the nonaxisymmetric impingement. Vaughan obtained solutions of the potential flow equations for the nonaxisymmetric case and showed that $C_{w,min} \propto Re_w$, which is consistent with the experimental results for the external-flow-dominated regime.

Similar results can be seen in Figures 10(b) and (c) for $G_c=0.01$ and 0.02. The benign effects of external flow are clearly visible at the smaller values of Re_w, particularly in Figure 10(c) where, for $Re_\theta=1.2\times10^6$, a value of $Re_w=0.4\times10^6$ reduces $C_{w,min}$ to approximately half the value required for zero external flow. Thus, correlations for $C_{w,min}$ with Re_θ in the absence of external flow are likely to be conservative at small values of Re_w/Re_θ but may produce underestimates at large values of this parameter. Figures 10(a), (b), and (c) also show that the extent of the external-flow-dominated regime increases with increasing G_c.

Comparative performance of the three seals

Although extensive flow visualization, pressure, and concentration tests were carried out for all the seals, complete results are only available for $G_c=0.005$ and 0.01. The three ingress criteria showed similar qualitative agreement and similar quantitative discrepancies for seals 3 and 5 to those discussed in the previous section for seal 1. For simplicity, only the results obtained using the flow visualization criterion are discussed below.

Figure 11 shows the effect of Re_w on the variation of $C_{w,min}$ with Re_θ for the three seals with $G_c=0.01$. For $Re_w/10^6=0.60$ and 1.17 in the external-flow-dominated regime, the differences between the seals are relatively small; for $Re_w=0$, in the

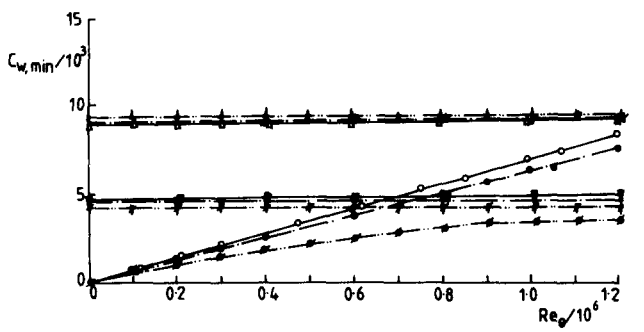

Figure 11 Comparison of the effects of Re_w on the variation of $C_{w,min}$ with Re_θ for seals 1, 3, and 5 with $G_c=0.01$ (according to the flow visualization criterion)

$Re_w/10^6$	0	0.60	1.17
seal 1	○	▽	△
seal 3	●	▼	▲
seal 5	◕	◥	◢

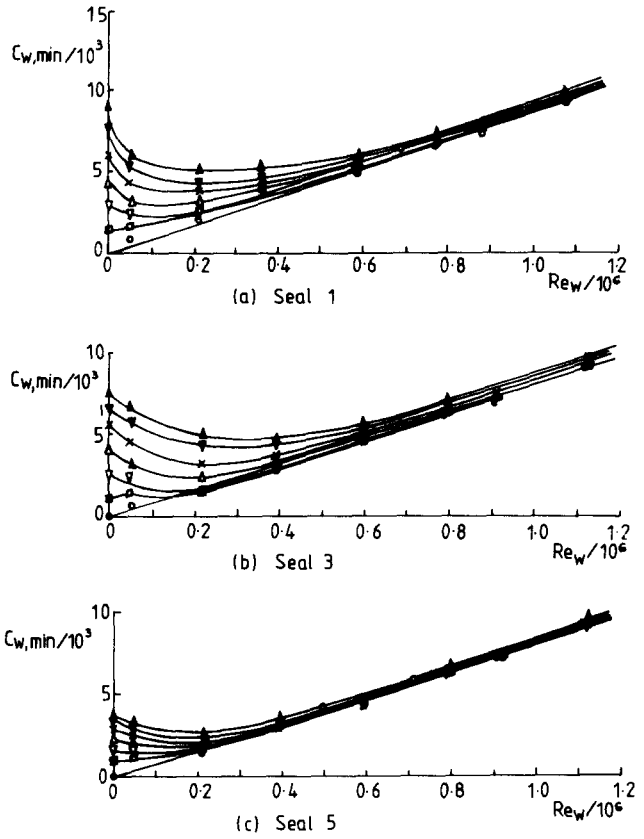

Figure 12 Comparison of the effects of Re_θ on the variation of $C_{w,min}$ with Re_w for seals 1, 3, and 5 with $G_c = 0.01$ (according to the flow visualization criterion): (a) seal 1; (b) seal 3; (c) seal 5

Symbol	○	□	▽	△	×	▼	▲
$Re_\theta/10^6$	0	0.2	0.4	0.6	0.8	1.0	1.2

rotation-dominated regime, the differences are much larger. In particular, seal 5 exhibits the nonlinear behavior associated with the pressure inversion effect discussed in I, and for $Re_\theta > 10^6$, $C_{w,min}$ appears to be virtually independent of rotational speed.

Figure 12 shows the effect of Re_w for each of the seals with $G_c = 0.01$. The transition from rotation-dominated to external-flow-dominated flow is clearly visible, and the "order of merit" for seal effectiveness is seal 5, 3, 1 for both regimes; seal 5 is also the most effective for $G_c = 0.005$. In the external-flow-dominated regime, the amount of cooling flow necessary to prevent ingress is only marginally less for seal 5 than for the other seals. However, it would appear from the concentration measurements shown in Figure 6 that, when $C_w < C_{w,min}$, the amount of fluid ingested into the wheel space will be significantly less for seal 5 than for the other seals.

Although the variation of $C_{w,min}$ with G_c, Re_θ, and Re_w could be correlated, the correlation would be misleading. In the external-flow-dominated regime, ingress is caused by pressure asymmetries rather than by Re_w itself, and, as stated above, the two were not independent for the tests reported in this paper.

Conclusions

In I, the effect of seal geometry on ingress in a shrouded rotor stator system operating in a quiescent environment was examined. In this paper, the effect of external flow on ingress is studied for three of the seals used in I (seal 1, the stationary shroud with an axial clearance between the rotor and the shroud; seal 3, the rotating shroud with an axial clearance between the stator and the shroud; seal 5, overlapping rotating and stationary shrouds with a radial clearance). Flow visualization, pressure and concentration measurements were used to determine $C_{w,min}$, the dimensionless sealing-air flow rate necessary to prevent ingress, for a range of rotational Reynolds numbers up to $Re_\theta = 1.2 \times 10^6$ and external-flow Reynolds numbers up to $Re_w = 1.2 \times 10^6$. The external flow was slightly nonaxisymmetric, with a maximum circumferential pressure difference (between any two of the 21 pairs of circumferential pressure taps) of approximately 7% of the dynamic pressure.

Although the flow visualization, pressure and concentration measurements produced qualitatively similar results, the pressure measurements tended to overestimate $C_{w,min}$. It was found that for all three seals there were two regimes: a rotation-dominated regime at small values of Re_w/Re_θ, and an external-flow-dominated regime at large values. For zero Re_w, $C_{w,min} \propto Re_\theta$ (apart from seal 5 in which the pressure inversion effect caused nonlinear behavior that reduced the increase of $C_{w,min}$ with increasing Re_θ). For small values of Re_w/Re_θ, increasing Re_w reduced $C_{w,min}$ for a given value of Re_θ: this was attributed to the sealing effect of an axisymmetric external flow. At large values of Re_w/Re_θ, $C_{w,min} \propto Re_w$ and the effect of Re_θ was insignificant: this behavior was attributed to the nonaxisymmetric pressure distribution in the external flow, which caused fluid to move transversely across the wheel space from regions of high to low pressure. For both regimes and for all seals and clearance ratios tested, $C_{w,min}$ increased with increasing clearance ratio, and $C_{w,min}$ was smaller for seal 5 than for the other seals.

In III, results are presented for tests conducted with a nonaxisymmetric external flow where the effects of the pressure asymmetry are separated from those of Re_w.

References

1 Phadke, U. P. and Owen, J. M. Aerodynamic aspects of the sealing of gas-turbine rotor-stator systems, Part 1: The behavior of simple shrouded rotating-disk systems in a quiescent environment. *Int. J. of Heat and Fluid Flow*, 1988, **9**(2), 98–105

2 Phadke, U. P. and Owen, J. M. Aerodynamic aspects of the sealing of gas-turbine rotor-stator systems. The effect of non-axisymmetric external flow on seal performance, Part 3: The effect of nonaxisymmetric external flow on seal performance. *Int. J. of Heat and Fluid Flow*, 1988, **9**(2), 113–117

3 Phadke, U. P. Aerodynamic aspects of the sealing of gas turbine rotor-stator systems. D.Phil. thesis, University of Sussex, 1982

4 Abe, T., Kikuchi, I., and Takeuchi, H. An investigation of turbine disc cooling (experimental investigation and observation of hot gas flow into a wheel-space). Paper No. GT-30, 13th CIMAC Conference, Vienna, 1979

5 Vaughan, C. A numerical investigation into the effect of an external flow field on the sealing of a rotor-stator cavity. D.Phil. thesis, University of Sussex, 1986